A Proposed Solution to the Range–Doppler Dilemma of Weather Radar Measurements by Using the SMPRF Codes, Practical Results, and a Comparison with Operational Measurements

JUHA PIRTTILÄ* AND MARKKU S. LEHTINEN

Sodankylä Geophysical Observatory, Sodankylä, Finland

ASKO HUUSKONEN

Finnish Meteorological Institute, Helsinki, Finland

MARKKU MARKKANEN

Eigenor Oy, Ltd., Helsinki, Finland

(Manuscript received 3 May 2004, in final form 10 April 2005)

ABSTRACT

Based on the measurement principles used on incoherent scatter radars, the authors have developed the Simultaneous Multiple Pulse Repetition Frequency (SMPRF) code that is intended to solve the range–Doppler dilemma and that can be used with modern magnetron radars. The working principle of the code is explained in mathematical terms and with the help of a simplified model. Results from the SMPRF and traditional fixed PRF weather radar measurements are compared, and the reasons for the differences are explained. The practical results show that the SMPRF code seems to work in the manner that is predicted by the theoretical and model calculations. The SMPRF code provides enough information to produce a high-resolution measured spectrum for each range gate. The shape of these measured spectra are seldom purely Gaussian. It is possible that more advanced raw products, other than just reflectivity, velocity, and width, can be produced with the help of these high-resolution spectra.

1. Introduction

The weather radar measurements, as used in the operational weather radar networks throughout the world, employ a uniform transmission of pulses. When measuring radar reflectivity, a low enough pulse-repetition frequency (PRF) (300–500 Hz) is used so that a transmitted pulse will leave the measurement volume before the next pulse is transmitted, providing an unambiguous reflectivity measurements result. The maximum measurement range $R_{\max}$ is calculated as

$$R_{\max} = cT/2, \tag{1}$$

where c is the velocity of the radio waves and T is the time separation between the adjacent pulses, that is, the inverse of the PRF. For example, for a PRF of 500 Hz the time separation between adjacent pulses is 2 ms and the maximum measurement range is 300 km without overlaid echo contamination.

When measuring wind speed, the time separation between adjacent pulses determines the maximum velocity $v_{\max}$ that can be unambiguously measured:

$$v_{\max} = \mathrm{PRF}\lambda/4, \tag{2}$$

where λ is the wavelength. At 5.6 GHz, a typical PRF of 1 kHz gives the maximum unambiguous velocity of 13.4 m s^{-1}.

These two equations show that as the PRF increases, the maximum velocity increases but the maximum unambiguous range decreases, and vice versa. In the lit-

* Deceased.

Corresponding author address: Markku Lehtinen, Sodankylä Geophysical Observatory, Tähteläntie 62, FIN-99600, Sodankylä, Finland.
E-mail: markku.lehtinen@sgo.fi

erature, this phenomenon is referred to as the "range–Doppler" dilemma or the range–velocity ambiguity (e.g., Doviak and Zrnić, 1993). There have been various attempts to overcome this problem (Sirmans et al. 1976; Laird 1981; Zrnić and Mahapatra 1985; Gray et al. 1989; Sachidananda and Zrnić 1999), but these papers have only been able to provide partial solutions.

Within other fields of radio science, radar methods have been developed that are not limited by the range–Doppler dilemma. Such methods have been presented, for example, by Farley (1972), Greenwald et al. (1985), and Lehtinen and Häggström (1987) for the ionospheric radar studies. However, these solutions are not directly applicable to the weather radar case. Yet, the coding methods that are used with the ionospheric radars give the tools for a possible solution of the dilemma. A solution was suggested in the Cooperation in Science and Technology (COST) 75 final seminar (Pirttilä et al. 1999), with an example of a code that could be used in practice and a simulation-based evaluation of the performance of the code. The name of the code is Simultaneous Multiple Pulse Repetition Frequency (SMPRF) (Lehtinen 2001). The solution is based on sending the pulses with changing intervals instead of having a fixed time separation between adjacent pulses.

Pirttilä et al. (1999) also evaluated the performance of SMPRF codes by a simulation approach. They concluded that, for measuring the reflectivity, an SMPRF code is as good as a traditional low-PRF pulse train. Regarding the velocity, they concluded that an SMPRF code would be able resolve high velocities without the need to limit the maximum measurement range.

In the present paper, we will describe in detail how an SMPRF code works, by showing both the exact mathematical formulation and a simplified example that has been worked through. We will then show radar reflectivity, radial velocity, and spectral width results based on the operational weather radar data that are based on fixed PRF codes and on the use of SMPRF codes. These data are measured almost simultaneously and, thus, they give a first evaluation of the SMPRF codes based on experimentally measured data.

2. Theory

a. Equations

A full radar measurement model, explaining the characteristics of the measured signal correlation products to the properties of a continuous and random scattering medium is presented in Lehtinen and Huuskonen (1996) for scattering from ionized plasma in the ionosphere. This is a distributed target similar to a weather target. There the concept of ambiguity functions is used to describe the way different ranges and different scattering times contribute to the estimates of the signal products when using complicated radar waveforms. In this article, we suppose very short radar pulses and the formalism becomes simpler, and, actually, no ambiguity functions need to be discussed. Instead, we derive the model relationship between our target and the samples obtained based on the simple physical arguments below:

First, because the range and time variables are very intimately connected in our method, we prefer to measure radar range by the time that is necessary for the radar pulses to do a trip to the target and back. When measured in time units, the distance is denoted by r, as opposed to distance in spatial units, denoted by R. Thus, $R = (c/2)r$.

We transmit pulses at time instances $t_i\Delta\tau$ and consider samples of them at time instances $t\Delta\tau$, where $t = 1, 2, \ldots, N$, and t_i is as sequence of (not necessarily consecutive) integers defining the pulsing of the radar. In our concrete example $\Delta\tau = 150$ μs, and we only consider samples at time instances 0, 150, 300, 450, ... μs. Similarly, we only consider scattering ranges r that are integer multiples of the same $\Delta\tau = 150$ μs. The reason for this is that only ranges corresponding to integer multiples of $\Delta\tau = 150$ μs can be related to the samples that are spaced in the same way.

This may not sound very practical, because one typically would sample at maybe a 1-μs sample rate. We actually also do this, but we rearrange the sample times and ranges that are considered into 150 different groups (labeled by an index $q = 0, \ldots, 149$) in the following way:

$$t\Delta\tau + q \times 1\mu s, \quad t = 0, 1, \ldots, 666, \quad \text{and} \tag{3}$$

$$r\Delta\tau + q \times 1\mu s, \quad r = 0, 1, \ldots, 19. \tag{4}$$

Thus, the considerations outlined below will actually have to be repeated 150 times, with each repetition dealing with 667 signal samples and target scattering behavior at 20 different ranges. (The number 667 comes from a typical rotation speed of a weather radar—rotating approximately the width of a radar beam in 100 ms $\approx 667 \times \Delta\tau$. The number 20 for the ranges corresponds to $20 \times \Delta\tau = 3000$ μs in range extent, approximately 450 km, which, in our weather conditions, guarantees that even a zero-elevation radar beam goes out from the atmosphere.) In theory, this separation of the problem into 150 mutually independent smaller problems is not at all necessary, but in practice it saves much computer time, because the solution of 150 equation sets of 667 equations with variables corresponding to the scattering behavior at 20 different ranges is much more efficient than the solution of one

equation set of 150 × 667 equations dealing with the unknown scattering behavior at 3000 ranges simultaneously.

The savings in the algorithm are explained in much more detail in the patent publication of Lehtinen (2001), and, in this paper, we now concentrate in the analysis of one group ($q = 0$) only. Restricting the study to the samples and ranges that are integer multiples of $\Delta\tau$ also serves the purposes of clarity in the explanation of the example case, as we can actually list all of the resulting equations.

A typical magnetron radar sends short pulses with random phases. We suppose, however, that, apart from the constant phase difference, the shapes of the pulses are otherwise the same. Let us choose one pulse as a "reference"; then, each pulse is the product of the reference pulse with a complex number of unit magnitude c_i. Let us denote the response from a scattering distance $r\Delta\tau$, received at time $t\Delta\tau$, be modeled by a coefficient $\sigma(r, t)$. This means that if a reference pulse would be sent at time $(t - r)\Delta\tau$, the signal sampled at time $t\Delta\tau$ would be given by $\sigma(r, t)$. However, instead of sending a reference pulse at time $(t - r)\Delta\tau$, we send a series of pulses at times $t_i\Delta\tau$ at random phases c_i, and the sampled signal z_t at time $t\Delta\tau$ is the sum

$$z_t = \sum_i c_i \sigma(t - t_i, t). \tag{5}$$

Let us denote the statistical expectation of a random signal by brackets $\langle\rangle$. Also, let us denote the complex conjugate by an overbar. It is well known that $\langle\sigma(r, t)\rangle = 0$, and that signals from different ranges are independent:

$$\langle\sigma(r, t)\overline{\sigma(r', t')}\rangle = 0, \quad \text{if} \quad r \neq r'. \tag{6}$$

It is then easy to derive the following equation for the signal power ($t = t'$):

$$\begin{aligned}\langle z(t)\overline{z(t)}\rangle &= \sum_i \sum_j c_i \overline{c_j} \langle\sigma(t - t_i, t)\overline{\sigma(t - t_j, t)}\rangle \\ &= \sum_i |\sigma(t - t_i, t)|^2.\end{aligned} \tag{7}$$

If the separations of the transmitted pulses at times t_i are shorter than the range extent of the target, several pulses contribute simultaneously to the signal power, and this formula can be used to model the relationship of the signal power $|z(t)|^2$ to the range-dependent scattering powers $|\sigma\ (t - t_i, t)|^2$.

b. Scattering lag estimates

Doppler measurements depend on lagged product estimates, where the signal sample corresponding to a certain range is correlated with another signal sample corresponding to the same range but measured at a differing time. We obtain estimates of scattering lags by considering estimates of the products of the signal with the complex conjugate of the signal sampled at another time:

$$\langle z(t)\overline{z(t')}\rangle = \sum_i \sum_j c_i \overline{c_j} \langle\sigma(t - t_i, t)\overline{\sigma(t' - t_j, t')}\rangle. \tag{8}$$

The expectation inside the double sum in (8) is nonzero only when the two range variables are equal:

$$t - t_i = t' - t_j \Leftrightarrow t - t' = t_i - t_j. \tag{9}$$

Thus, we will get estimates of scattering lags for all of those lag values that correspond to separations of two pulse locations in the transmitted pulse chain. It is also rather easy to choose the transmitted pulse chains in such a way that two different ranges never simultaneously contribute to the sum in (8), as is shown in the illustrations of the following section.

c. Noise

There is good reason to ask whether the idea of solving (7) would break down in the case where we have huge differences of scattering power at the different ranges that are involved in the sum of (7).

Similarly, in using (8) we are well aware of the fact that while the unwanted multitrip echoes do not cause a contribution to the expected values of the signal products, they appear as noise in the resulting lag estimates.

We must admit that we do not fully understand how noise works in these kinds of situations, and much more work is necessary to gain this understanding. We have done much research on the effects of noise for incoherent scatter radars (see, e.g., Huuskonen and Lehtinen 1996; Lehtinen et al. 1997), but this work is certainly not directly applicable to weather radar. In that process, we have learned that it is of the utmost importance to consider full-noise models, including the effects of correlations of different noise components, especially in case of high signals. We have also learned that those correlations, when properly taken into account, do not necessarily worsen the situation; they may easily lead to unexpected improvements in the accuracy of the desired results.

With regard to weather radar, we can mainly refer to the practical results shown later in the present paper, which give no reason to suspect that noise would destroy the idea promoted here. The simulations in Pirttilä et al. (1999) for SMPRF in weather radar also suggest this.

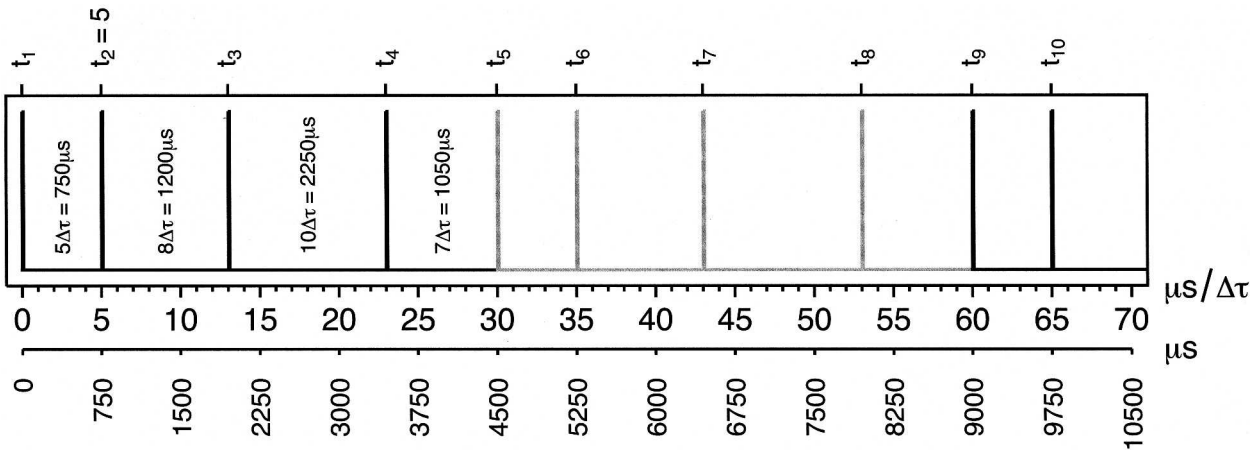

FIG. 1. An illustration of the code used together with various notations that describe the code timing. In our example the basic time unit is $\Delta\tau = 150$ μs, and all of the pulse positions t_i are multiples of it. We have marked the first four pulse intervals between the pulses in the figure. The sequence repeats itself in intervals of 30 time units ($30 \times \Delta\tau = 4500$ μs), and we have drawn the first repeated series of pulses in gray.

As a theoretical explanation to this seemingly favorable behavior we want to note the following:

Regarding huge differences in scattering power at different ranges in (7), we first note that this itself is no problem, at least if we can suppose that the radar sampling system works linearly. In statistical inversion, a huge value of one unknown does not change the error estimate for another unknown! Only the error values of the data side of the equations count here, making the problem similar to the other question about errors caused by multitrip echoes in the lag estimates.

The noise that is caused by multitrip echoes in the lag estimates can indeed be very high in many lags. However, because we estimate many different lags, and because the multitrip noise comes from different ranges in those different lags, there usually are also many lags that are available where the errors are not high. This same applies for the multitrip noise in solving the power equations: some of the equations may have high errors and some not. Because statistical inversion solutions automatically properly weight the different data in the equations, those parts of the data having high errors do not affect the solutions and the errors in the solutions tend to correspond to that part of the data that happens to have the smallest errors.

3. An example

a. The code

We next continue our example to illustrate the SMPRF concept. For this purpose, let us assume a very simple code that contains only four different pulse separations: 5, 8, 10 and 7 time units (already illustrated in Fig. 1). The sum of the separations is 30, which means that the code repeats in steps of 30 time units. One time unit is 150 μs, repeating the example of the previous chapter.

Assume now that samples are taken at 1 time unit apart, and that the longest distance producing significant scatter is 20 time units. The range of 20 units would correspond roughly to 450 km in distance. This range is generally considered to be far enough so that even a horizontally sent pulse is above the weather and, thus, the pulses beyond 20 time units do not produce any signal.

Figure 2 shows that at time instant 31 the pulse that is sent at time 30 is at a distance of 1 unit, and the previous pulses are at distances of 8, 18, and 26. Thus, the signal that is recorded represents a sum of a first-trip echo from the distance of 1, and second- and third-trip echoes from distances of 8 and 18. We can neglect any previous pulse because of the assumption that no significant scatter is obtained from a distance greater than 20 units. The pulse locations are given in Table 1. Figure 2 shows the pulse locations for sampling times of 31, 36, 47, and 52. Because no data can be recorded when a pulse is being sent, there will be no data from times 35, 43, 53, and 60.

b. The reflectivity data

The power values are obtained by squaring the signal samples and averaging them over the integration period. (We further reduce the computational burden from the figures that are outlined in the previous sec-

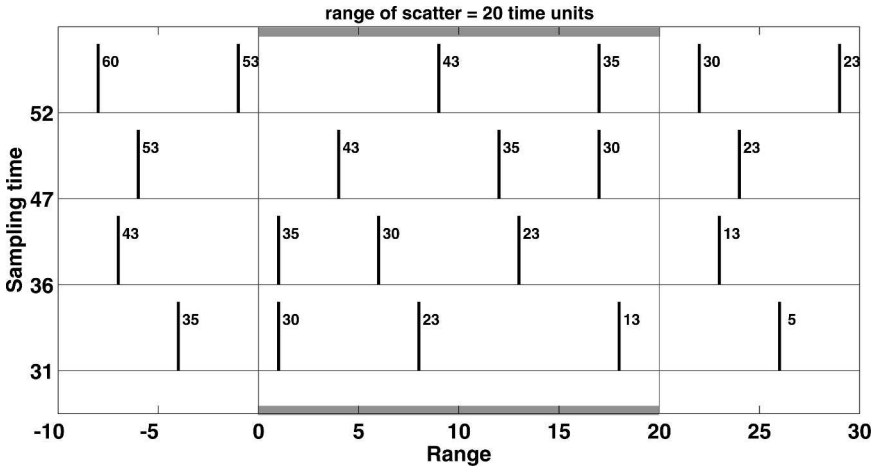

FIG. 2. Pulse locations at four time instances (31, 36, 47, and 52 time units).

tion by using the repetitive nature of the measurement by summing up corresponding signal products every $30\Delta\tau$, which is the period of the repetition of the pulse pattern. This summation is called time integration.) Thus, the pulse location as given in Table 1 also gives the contribution ranges in the power estimates in accordance with (7). It is seen that the power estimates are ambiguous because they represent sums of powers at many ranges. A closer look at the numbers shows that the combinations of ranges are different at each time instant. Thus, we may form a set of linear equations, where we have 26 equations and 20 unknowns, and can solve for the power at each range. The number of equations is less than 30, because there are four time instants when a pulse is sent and no data are recorded. In this way, we obtain an unambiguous power profile from the ambiguous observations. This procedure is called as the zero-lag inversion.

It is instructive to compare the solution with the solution that is possible when using standard weather radar coding. A similar case appears when velocity is measured with standard Doppler weather radars; the pulses must be sent so close to each other that the power values are not usable. However, the solution that is presented above is not possible, because each range appears always in an identical combination of ranges. This is caused by the fact that the pulse separation is fixed. We note that the matrix that is defined by the linear problem for a fixed PRF code is singular, and the problem is ill posed.

c. The I and Q signals

A Doppler velocity estimate requires that we measure in-phase and quadrature samples of the signal. We can conveniently combine the I and Q samples together to form a complex sample $x_t = I_t + iQ_t$. In standard weather radars, the phase angle is determined relative to the transmitted pulse, but it may also be determined relative to a fixed free-running sampling clock.

An estimate of the autocorrelation function (ACF) at a lag value is obtained by multiplying two complex samples together, and averaging over a chosen integration time. Now, take samples x_{31} and x_{36} as examples. As seen from Table 1 and Fig. 2, the first sample gets contributions from ranges of 1, 8, and 18, and the second from ranges of 1, 6, and 13. The important thing to note is that scattering from two different scattering volumes does not correlate in the statistical sense. Thus, the product $x_{31}\overline{x_{36}}$ gets a statistical correlation from range 1, with the scattering from other ranges only appearing as noise. When the same measurement is repeated and the products are averaged, the expected value of the product is the estimate of the autocorrelation function at range 1, with a time delay of five time units. The pulse locations for range 17 are shown in Fig. 2. We see that the noncontributing pulses are now lo-

TABLE 1. Locations of the contributing pulses for sampling times 31–60.

Time	Ranges	Time	Ranges	Time	Ranges
31	1, 8, 18	41	6, 11, 18	51	8, 16
32	2, 9, 19	42	7, 12, 19	52	9, 17
33	3, 10, 20	43	No data	53	No data
34	4, 11	44	1, 9, 14	54	1, 11, 19
35	No data	45	2, 10, 15	55	2, 12, 20
36	1, 6, 13	46	3, 11, 16	56	3, 13
37	2, 7, 14	47	4, 12, 17	57	4, 14
38	3, 8, 15	48	5, 13, 18	58	5, 15
39	4, 9, 16	49	6, 14, 19	59	6, 16
40	5, 10, 17	50	7, 15, 20	60	No data

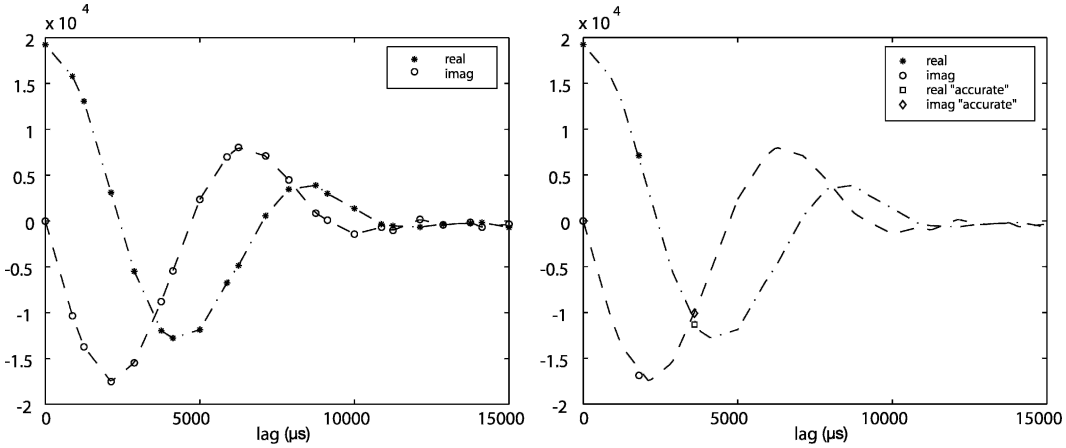

FIG. 3. Autocorrelation samples from a (left) SMPRF code and (right) traditional measurement with fixed 570-Hz PRF.

cated at closer ranges than the pair-producing correlation. This does not hamper the determination in any other way than by the fact that the signal from the noncontributing pulses may be strong relative to the contributing pair.

We will get a statistical contribution for any lag value, which corresponds to any pulse separation in the code. These include, in our case, 5, 7, 8, 10, 12, 13, 17, 18, 20, 22, 23, 25 and so on. For each of these lags the processing is the same as that in a traditional pulse-pair method. The main differences here are that 1) each possible pulse pair within the code is used for the autocorrelation estimates and 2) the extended pulse-pair processing is carried out to a maximum range of the code, not just the range defined by the shortest pulse separation of the code.

4. Moment estimation of SMPRF measurements

The pulse-pair processing of the fixed PRF weather radar data produces only two complex samples of the autocorrelation function of the weather signal (Doviak and Zrnić 1993). The moment estimation is straightforward; the signal power is interpreted as the radar reflectivity. The velocity is obtained directly from the first lag, and the spectrum width is usually obtained from zeroth and first lag, but an algorithm using the second lag exists as well (e.g., Sigmet, Inc. 2000).

On the other hand, one can easily see that an SMPRF code consisting of n pulses produces $n(n-1)/2$ nonzero-lag samples of the autocorrelation function of the weather signal and the zero-lag inversion produces the power estimate. Thus, altogether we get $n(n-1)/2+1$ autocorrelation samples using the SMPRF code. This fact is illustrated in Fig. 3. The left panel of the figure shows the 22 estimates obtained from a seven-pulse SMPRF code. The right panel of the figure shows the three autocorrelation samples from the traditional measurement with fixed 570-Hz PRF. The autocorrelation function of the weather signal is sketched in both panels using dashed lines.

The irregular set of lags defines the unambiguous velocity span for the code. The absolute maximum for the velocity span of the code can be simply calculated from the smallest difference between the lags by applying (2). The velocity span of the SMPRF codes that is used in our practical measurements was always better than about $-50 \ldots +50$ m s^{-1}, which was certainly enough in our climate.

Because the SMPRF code produces a large number of autocorrelation samples, we cannot estimate the moments of the spectrum using simple direct methods. Instead, we fit, within the velocity span of the code, a Gaussian ACF to the measured samples. The parameters of the ACF that best fits to the measured autocorrelation samples are used as the estimated spectral moments.

Most of the time, especially in the rain cases, the Gaussian assumption seems to be acceptable and the measured autocorrelation samples fit well to the Gaussian model. The left panel of Fig. 3 shows an example of such a set of autocorrelation samples. However, in many cases, the measured autocorrelation samples do not fit well to the Gaussian model (an example of such a non-Gaussian set of autocorrelation samples is shown in the left panel of Fig. 8).

The differences between the SMPRF-produced spectrum parameters and the Interactive Radar Information System (IRIS)-produced spectrum parameters raise a need to investigate the true spectra of the

SMPRF-measured autocorrelation samples. The method to obtain these spectra is explained in the following.

The power spectrum is a Fourier transform of the autocorrelation function. From the SMPRF code the autocorrelation function is obtained but, because of the irregular pulse intervals in the SMPRF code, the autocorrelation samples have also irregular intervals. This problem can be overcome by treating the Fourier transform as an ill-posed inversion problem. Statistical inversion is our tool here. The measurement of irregularly sampled ACF is modeled as

$$\mathbf{m}_{\mathrm{ACF}}(\tau) = \mathbf{A}\mathbf{S}(\omega) + \boldsymbol{\epsilon}, \tag{10}$$

where $\mathbf{m}_{\mathrm{ACF}}$ is the vector of measured autocorrelation samples at lag values τ, $\mathbf{S}(\omega)$ is the vector spectrum value within the desired Doppler frequency range ω, $\mathbf{A}$ is the theory matrix containing the coefficients of the inverse Fourier transform, and $\boldsymbol{\epsilon}$ is the noise.

Because we want to calculate high-resolution spectra, we must increase the resolution of the Doppler frequency axis ω. By doing this, we increase the number of unknowns and the problem becomes ill posed. We can solve this ill-posed problem by taking into account the a priori knowledge about the possible values of our unknown variables, which, in this case, is the following three conditions: 1) that the values of $\mathbf{S}(\omega)$ are nonnegative, 2) that the neighboring values of $\mathbf{S}(\omega)$ do not differ much, and, last, 3) that the values of $\mathbf{S}(\omega)$ are zero outside the ω grid. A much more thorough discussion about solving linear and nonlinear inversion problems with statistical inversion can be found in Kaipio and Somersalo (2004), Evans and Stark (2002), Mosegaard and Sambridge (2002), Vallinkoski and Lehtinen (1990), Lehtinen (1988), and Kaipio et al. (2000).

5. The SMPRF code compared with dual-PRF and dual-PRT techniques

The SMPRF code resembles the well-known traditional dual-PRF/-pulse-repetition time (PRT) approach that is commonly used to reduce velocity ambiguities. There are a number of essential differences between the methods, which are discussed in the following.

The concept extending the unambiguous velocity by using two different sampling rates was first suggested by Sirmans et al. (1976). There are two possible variations of this technique: dual-PRF and dual-PRT. Both rely on using two different PRTs. In both methods, the unambiguous range is the range of the shorter of the PRTs. If the unambiguous range of the dual-PRF/-PRT measurement is too short, second-trip echoes will become a problem. The dual-PRF/-PRT techniques do not provide any mitigation to this part of the range-Doppler dilemma.

In the dual-PRF technique, the radar sends pulses with two alternating PRFs—one ray with a high PRF and the next with a low PRF. By combining the velocity measurements at the two PRFs, the unambiguous velocity interval can be extended. It is common practice to choose the low and high PRFs in such a way that

$$\frac{\mathrm{PRF}_{\mathrm{high}}}{\mathrm{PRF}_{\mathrm{low}}} = \frac{N+1}{N}, \tag{11}$$

where N is the factor by which the maximum unambiguous velocity is extended. The dual-PRF technique has been implemented in many radars worldwide.

In the dual-PRT technique the pulses are spaced at alternating PRTs T_1 and T_2, $T_1 < T_2$. The pulse-pair processing is then done independently for each PRT, and the estimates are suitably combined so that the maximum unambiguous velocity becomes $V_u = \lambda/[4(T_2 - T_1)]$ (Zrnić and Mahapatra 1985). The dual-PRT technique has been very rarely implemented in weather radars because of the difficulties in designing efficient ground clutter filters.

When the dual-PRF/-PRT technique is considered as a way to sample the ACF, the essence of both of these techniques is to provide one more autocorrelation sample when compared with the traditional single-PRF technique. Figure 4 shows the autocorrelation samples that are provided by a high-PRF ray of a dual-PRF measurement with PRFs 570 and 380 Hz (3:2). It is worthwhile to note that in Fig. 4 the autocorrelation sample at second lag (2700 μs) comes from different volume from the rest of the lags. This is an additional source of error for the dual-PRF technique, because the actual velocities in the neighboring rays are not necessarily close enough to each other. In the dual-PRT technique, all of the autocorrelation samples are from the same volume, and this slight problem does not exist.

The estimation of the velocity is based on differencing the lags 1 and 2. It is evident, that the noisier and closer (in lag) to each other these autocorrelation samples are the more uncertain is the dual-PRF velocity estimate. In practice, the dual-PRF/-PRT velocity estimate is merely used to indicate to which Nyquist interval the original folded velocity estimate belongs.

In the dual-PRF algorithms that are used today, the spectral moments are estimated exactly the same way they are estimated in the traditional single-PRF technique. The difference between first and second lag is used only to find the correct Nyquist interval for the folded velocity (e.g., Sigmet, Inc. 2000).

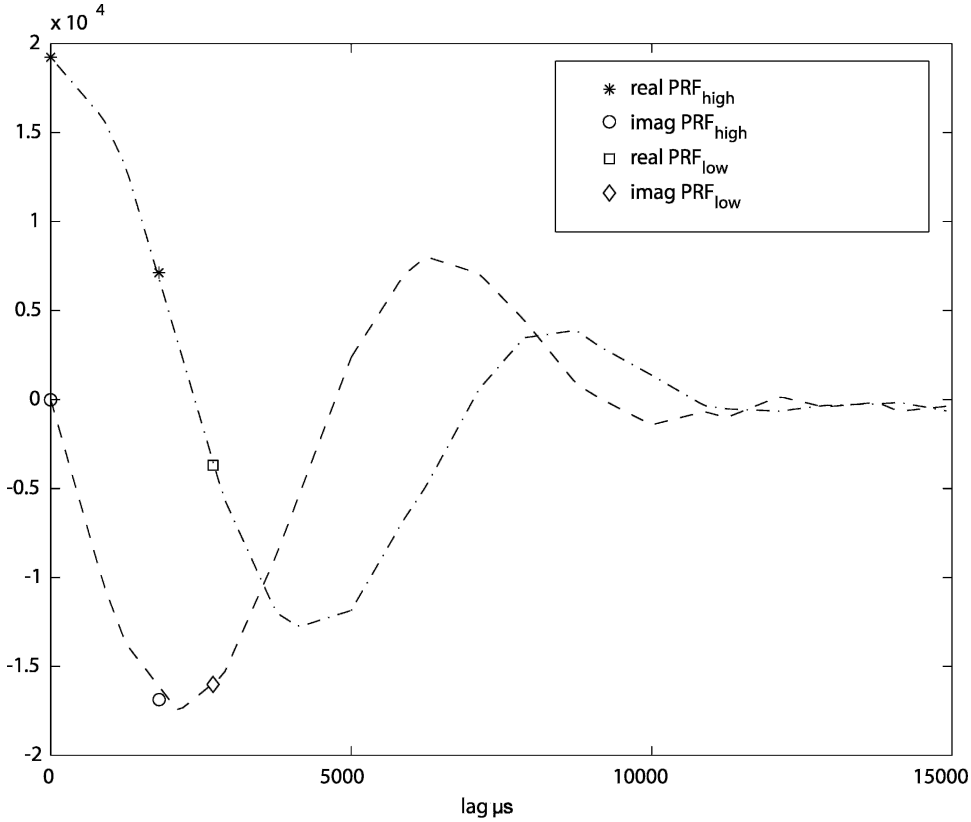

FIG. 4. Autocorrelation samples from a dual-PRF measurement, with a high PRF = 570 Hz and low PRF = 380 Hz.

The differences between the dual-PRF/-PRT techniques and the SMPRF code are as follows:

- The autocorrelation samples are calculated for a large number of range gates, well to the traditional second- or third-trip domain. All the possible pulse pairs within the code are used for the autocorrelation samples.
- The SMPRF code provides the much larger number of autocorrelation samples, and they are all from the same volume.
- The higher number of irregularly sampled autocorrelation samples makes the expansion of the unambiguous velocity interval much more reliable than just relying on the difference between lags 1 and 2.
- Second-trip echoes are generated on purpose; the zero-lag inversion provides the unambiguous reflectivity profile.
- The spectral moments are estimated by fitting a Gaussian autocorrelation function to the measured autocorrelation samples instead of simple direct methods.
- Large number of autocorrelation samples enables the investigation of the true power spectra of the weather signal for each range gate.

6. Practical results

a. Measurement setup

The Finnish Meteorological Institute (FMI) operates a weather radar on top of the Luosto fell (67°8′N, 26°54′E; 514 above MSL). The Luosto radar is a C-band weather radar with a 250-kW magnetron transmitter built by the German radar manufacturer Gematronik. In the operational use, the transmitter is controlled by the Sigmet RVP7 signal processor, and the signal is processed and analyzed by Sigmet's IRIS software. The Luosto radar is also used for the development of new radar coding methods, based on the Invers, Ltd., Grand Unified Radar Signal Processor (GURSIP) solution. During these measurements, the GURSIP solution handles the transmission of the SMPRF codes, the sampling of the signal [at 30 MHz intermediate frequency (IF)], and the sampling of the pulse forms, the detection of the signal, and first stages of the signal processing. From the GURSIP card the data are transferred over the peripheral component interconnect (PCI) bus to a powerful reduced instruction set computer (RISC) workstation running Berkley

Software Distribution (BSD) UNIX. During the measurements discussed in this paper, the radar workstation only stored the detected signal to a hard disk. The rest of the signal processing and data analysis was performed afterward by another workstation offline.

The measurements with these two signal-processing systems are arranged so that almost simultaneous measurements are available for comparison. The actual time difference is 2 min. In the following, the results based on the Sigmet IRIS system will be called FMI or operational results and the results based on the Invers, Ltd., development equipment will be called the SMPRF results.

The data for this study were collected at the Luosto radar in the morning of 21 August 2003. The measured weather consisted of a front with some precipitation extending in the southwest–east direction about 220–290 km from the radar. The wind was not very spectacular; the maximum speed was 17.5 m s^{-1}, which is still high enough to cause problems for the operational measurement.

During this event, and also throughout the summer of 2003, the SMPRF solution was based on 2-μs pulses, with an effective PRF of 480 Hz. Three pulses were used in the cycle, which was 6250 μs long. The separations between the pulses were 1750, 2000, and 2500 μs, making the greatest common divisor $\Delta\tau = 250$ μs.

The maximum range for the SMPRF measurement was 300 km, and the velocity span was from -53 to 53 m s^{-1}. In the SMPRF method, both the maximum range and the maximum velocity can be freely chosen, but in practice we are constrained by the limitations that are posed by the transmitter and the receiver performances. The operational FMI scan was a standard pulse train of 2-μs pulses (PRF 570 Hz), having the maximum range of 250 km and the folding velocity of 7.5 m s^{-1}. In both cases the antenna rotated with a speed of 10° s^{-1}, and the elevation angle was 0.1°. The angular resolution was the standard 1°, and, thus, each ray was measured in 0.1 s.

b. Reflectivity results

Figure 5 shows the results from both the operational and the SMPRF scan. All of the figures have the same scale: the maximum range is 300 km. Because of the difference in maximum ranges of the measurements, the operational results are shaded with gray beyond the 250-km range. In addition, we have drawn a light gray circle on the SMPRF images to help to distinguish what is unseen at the far ranges in the operational scan. The dark gray circles denote the 100-km-range intervals.

The top row of the Fig. 5 shows the radar reflectivity results. The precipitation area is oriented mostly in an east–west direction, extending about 270 km to the east and 220 km to the southwest. In the north–south direction the dimension of the precipitation area is about 100 km. The reflectivity fields are strikingly similar despite the 2-min time difference between the scans. The top panel of Fig. 6 compares reflectivity profiles from both scans at the azimuth of 225°. One can clearly see that both curves "walk hand in hand" and the differences are most probably a result of the time difference between the scans.

Figure 7 shows details of the reflectivity fields of the operational and SMPRF scans. The dBZ field of the operational scan contains holes, whereas the holes are absent in the SMPRF reflectivity field. The holes appear at ranges with strong ground clutter, which can be seen in total echo power (dBT), shown in the middle panel of Fig. 7.

c. Velocity results

The middle row of Fig. 5 shows velocity results from both scans. The velocity results of the operational scan are between -7.6 and 7.6 m s^{-1}, which are consistent with the folding velocity of 7.6 m s^{-1} of the operational measurement used. It is evident that the velocity values are folded and ambiguous. The velocity results of the SMPRF scan are between -16.4 and 17.5 m s^{-1}, and no folding has appeared. The SMPRF results are clearly unambiguous.

The middle panel of Fig. 6 compares velocity profiles from both scans at the azimuth of 225°. Velocity profile from the SMPRF code shows unambiguous velocities between 1.7 and 11.7 m s^{-1}, whereas the velocity profile from the operational scan is partly folded.

The velocity profile from the SMPRF code shows a steep step at the 50-km range. Similar steps or small spikes can be seen in the velocity profile at ranges beyond 100 km. The reason for these steps and spikes can be understood by examining the ACF data that are produced by the SMPRF code. The right panel of Fig. 8 shows the power spectrum, which is the Fourier transform of the autocorrelation samples on the condition that the spectrum is nonnegative. The spectrum clearly reveals that the scattering volume contains four wind velocity peaks.

Our fitting procedure fits a Gaussian ACF around the velocity that has the most power within the scattering volume. If there are two almost equally strong wind velocity peaks, the fitted velocity can jump sharply from gate to gate as the fitting procedure chooses the stronger of the two at each gate. This explains the steps and small spikes that are seen in the velocity profile. Figure 9 shows both the spectra calculated directly from

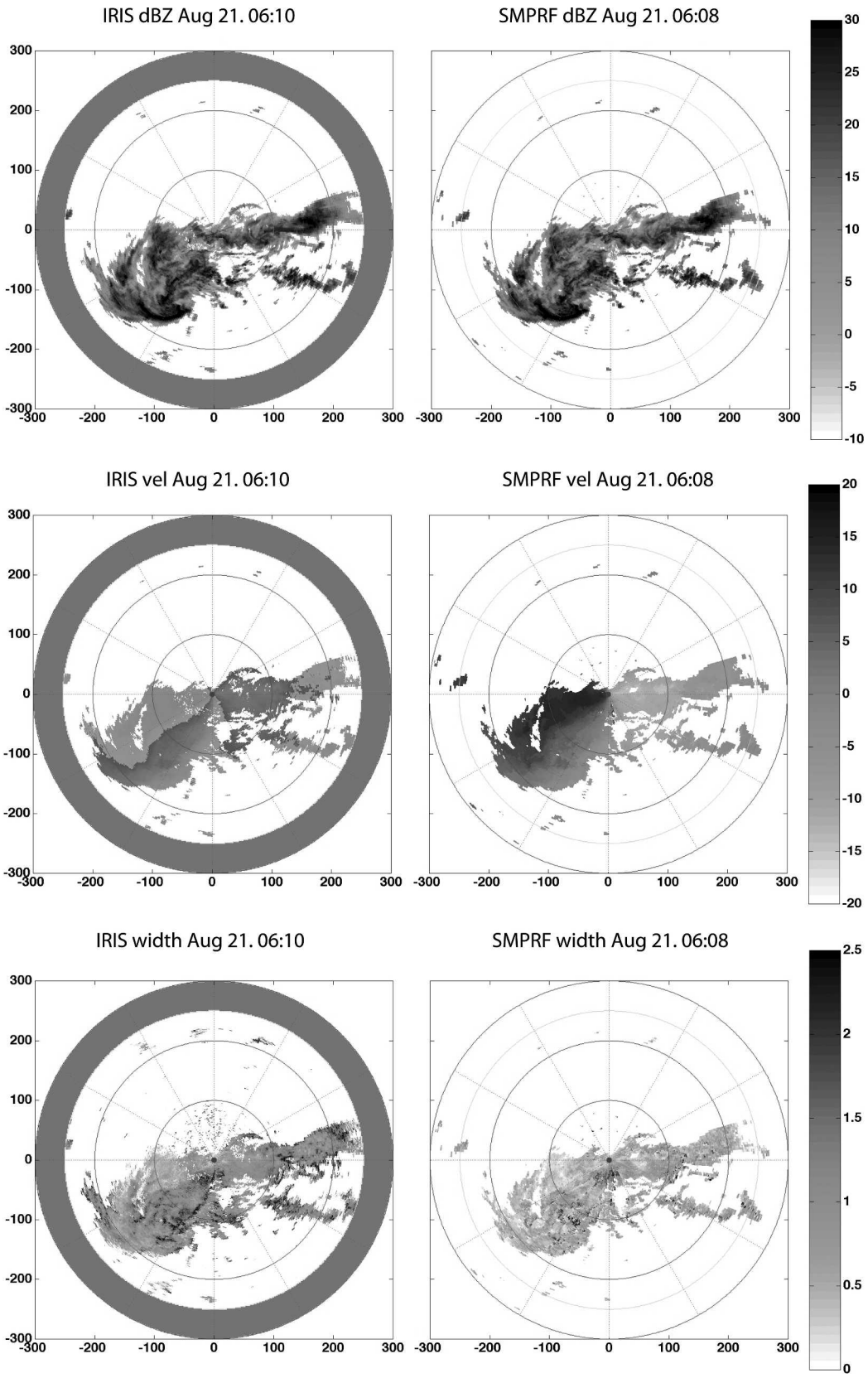

FIG. 5. Results from the (left) operational and (right) SMPRF scans.

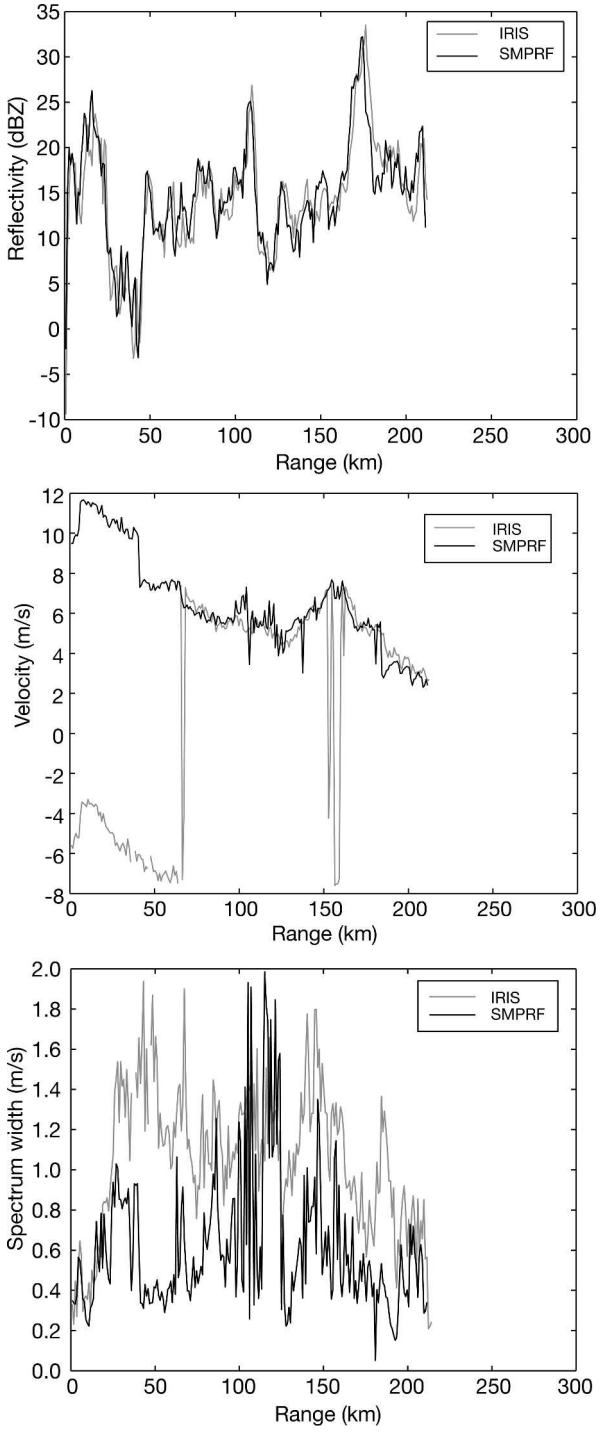

FIG. 6. Parameter profiles from IRIS and SMPRF at azimuth 225°: (top) reflectivity, (middle) velocity, and (bottom) spectrum width.

the autocorrelation samples and the spectra calculated from the fitted Gaussian ACF at nine different ranges from 34.1 to 55.7 km. The steep step in our example profile appears at 42.2 km, where the SMPRF velocity estimate jumps from 10 (higher velocities) to 7.5 m s^{-1} (lower velocities). The spectra that are calculated from the autocorrelation samples show that the lower velocities are present in the signal already at the 34.1-km range, and that their power becomes larger than the power of the higher velocities at the 42.2-km range. The higher velocities are still visible in the spectra at the 55.7-km range. The fitting procedure fits an ACF around the velocity that has the highest power, and the step is formed at the 42.2-km range.

d. Spectral width

The bottom row of Fig. 5 shows spectrum width results from both scans. The width results of the operational scan are less than 4.7 m s^{-1}. The width results of the SMPRF scan are less than 3.7 m s^{-1}, and in many places are smaller than the width estimates from the operational scan. However, the results are closely identical at places. For example, there is a continuous area of larger widths just south of the radar at 10–40-km ranges.

The bottom panel of Fig. 6 compares width profiles from both scans at the azimuth of 225°. For ranges from 25 to 90 km, the SMPRF widths are significantly smaller than the widths from the operational scan.

Because the full spectrum from the operational scan is not available, any explanation for this and other differences in the width estimates can only be given by examining the ACF data that are produced by the SMPRF code and by calculating spectral estimates with various methods.

For this purpose, we can use the almost Gaussian ACF (shown in the left panel of Fig. 3) and the clearly non-Gaussian case (shown in the left panel of Fig. 8). Spectrum parameters are analyzed from both ACFs using the following two methods: the fitting and the direct parameter estimation.

The direct parameter estimation methods used by IRIS are applicable only when the autocorrelation samples are calculated from an evenly spaced pulse train. To enable the use of these simple direct methods, the autocorrelation samples at lags 0, 1800, and 3600 μs were interpolated from the original SMPRF-generated samples by spline interpolation. These values are denoted by triangles in the autocorrelation panels of the Figs. 10 and 11.

The real shape of the spectrum was calculated directly from the autocorrelation samples using the statistical inversion analysis presented above. In addition, to get the SMPRF estimate of the spectrum parameters, a Gaussian autocorrelation function was fitted to the autocorrelation samples using the Levenberg–

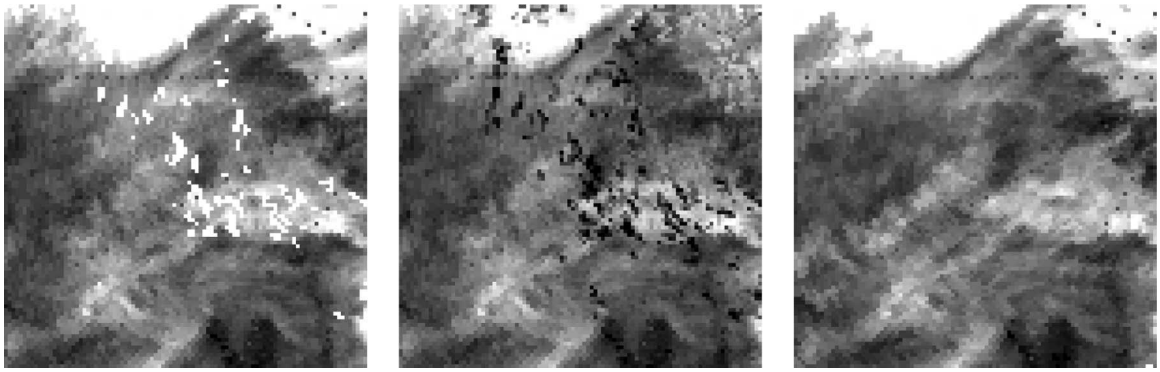

FIG. 7. Enlarged reflectivity fields at about the 10–80-km range west-southwest from the radar: (left) dBZ of the FMI scan, (middle) dBT of the FMI scan, and (right) dBZ of the SMPRF scan.

Marquardt algorithm. The fitted ACF is denoted in the left panels of Figs. 10 and 11 by dashed lines. Last, two IRIS estimates of the spectrum parameters were calculated from the three interpolated lags using the direct methods that were presented in the IRIS user's manual. From these parameters three Gaussian spectra were calculated—SMPRF fitted, IRIS "accurate," and IRIS "fast"—and were plotted together with the measured spectrum in the right panels of Figs. 10 and 11.

Figure 10 shows that when the measured autocorrelation samples fit well to the Gaussian spectrum model and the noise is small relative to the values of the autocorrelation estimates, all of the methods to estimate the width of the spectrum produce very similar results. The width estimates are 0.84 m s^{-1} for the IRIS accurate method, 0.74 m s^{-1} for the IRIS fast method, and 0.88 m s^{-1} for the SMPRF fit. The operational FMI scan that was performed 2 min later provided a width of 0.82 m s^{-1} for the same ray and range.

As soon as the autocorrelation samples deviate slightly from the Gaussian spectrum model, the direct methods to obtain the width estimate start to produce wrong results. Figure 11 shows a typical non-Gaussian form of the ACF. In the measured data, this type of ACF appears for several tens of kilometers in range and several neighboring rays, so the signal must come from the weather. Typically, in most of the non-Gaussian cases the short lags between 1000 and 5000 μs have smaller absolute value than the longer lags, and, therefore, the direct estimates produce a large width. For the same reason the velocity estimates also deviate from each other.

In the non-Gaussian case the Levenberg–Marquardt fitting that was used in the SMPRF analysis finds the strongest velocity peak of the spectrum. The velocity estimate is then the velocity where most of the power is. The width estimate becomes narrower than the width of the highest velocity peak. The reason for this is that Gaussian ACF tends to fit to the non-Gaussian autocorrelation samples in a way that produces a wide ACF and, thus, a too narrow Gaussian spectrum.

The width estimates in the non-Gaussian case are 1.3

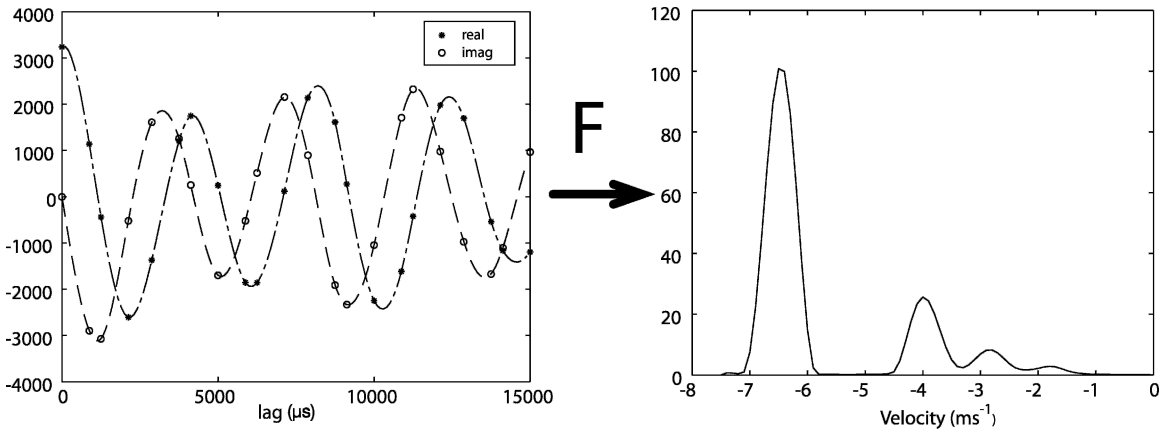

FIG. 8. (left) Measured autocorrelation samples and (right) the corresponding spectrum.

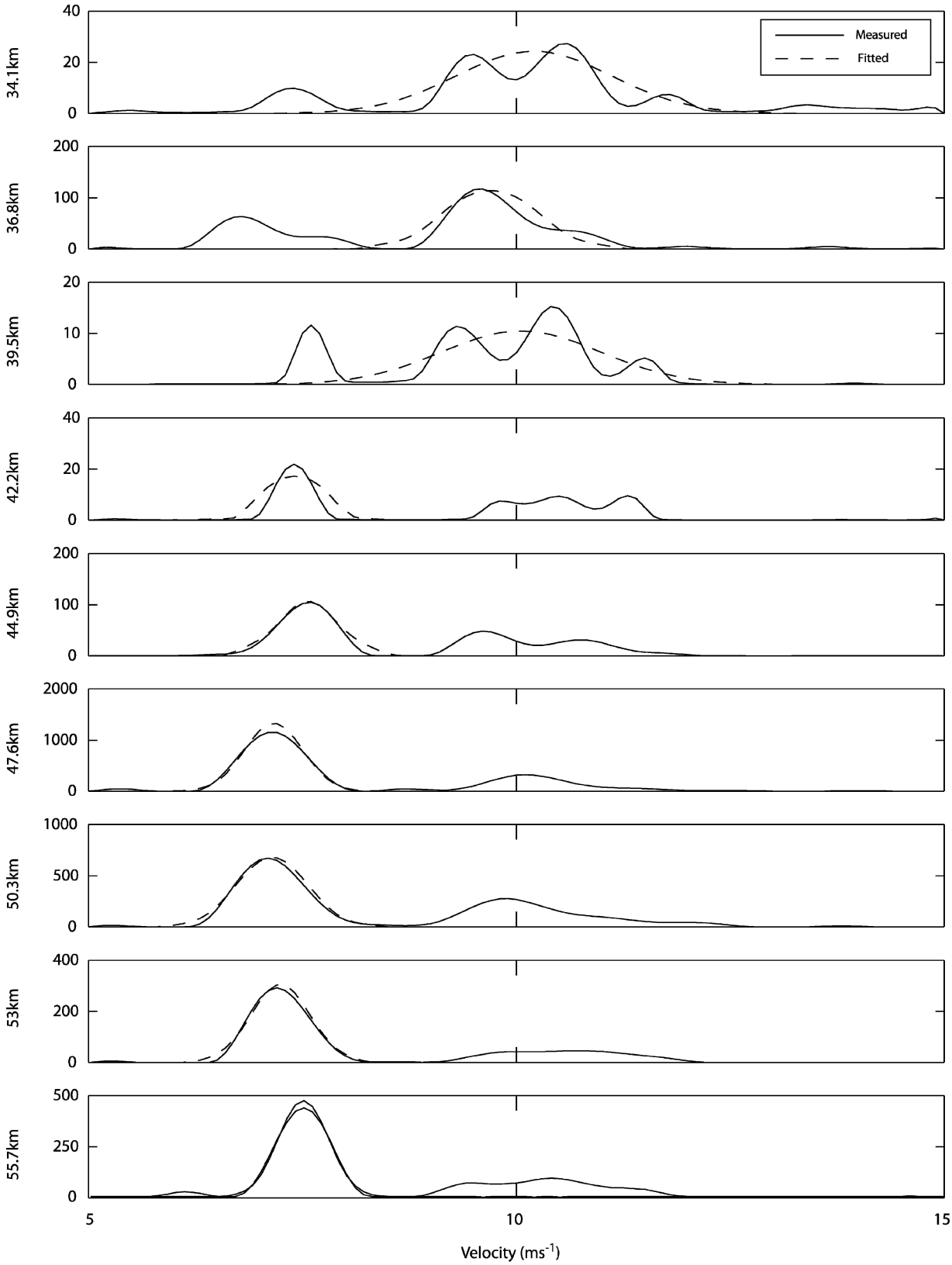

FIG. 9. Spectra calculated from measured ACFs by the statistical inversion method compared with Gaussian spectra fitted to the autocorrelation samples for ranges from (top) 34.1 to (bottom) 55.7 km.

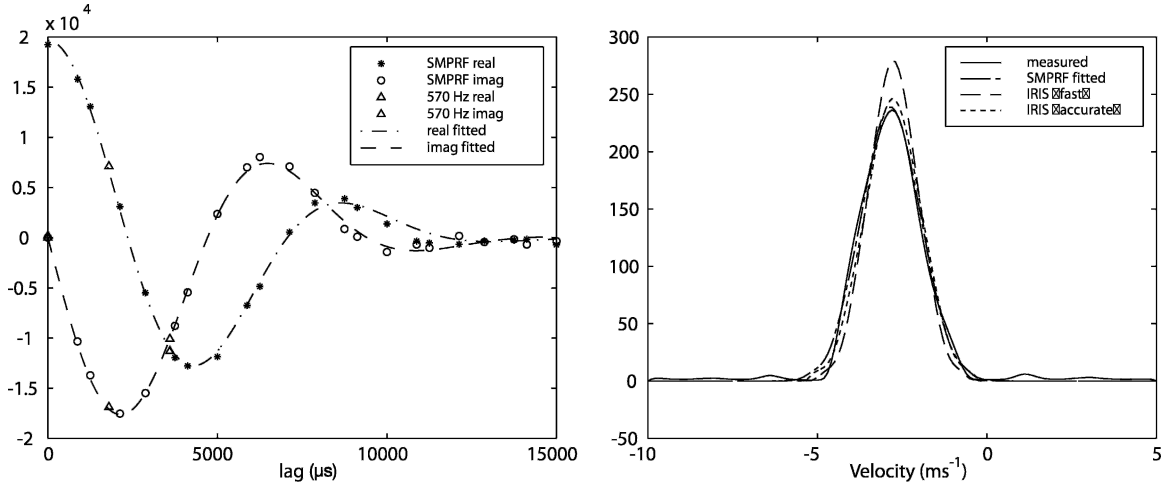

FIG. 10. (left) Measured autocorrelation samples that fit well to the Gaussian spectrum model, and (right) the corresponding spectrum and spectra of different analysis results.

m s^{-1} for the IRIS accurate method, 1.4 m s^{-1} for the IRIS fast method, and 0.23 m s^{-1} for the SMPRF fit. The operational FMI scan that was performed 2 min later provided a width of 1.3 m s^{-1} for the same ray and range.

7. Discussion and conclusions

The results of this paper suggest that the proposed SMPRF technique is effective in mitigating the range–velocity ambiguity problem. The solution is based on using radar coding where we send series of pulses that are irregularly spaced and so close to each other that echoes from different ranges in the target are received simultaneously. However, unique results for the reflectance and correlation estimates from each range are obtained by statistical inversion techniques. This method allows us to choose freely both the maximum range to be measured and the maximum velocity to be determined, and there is no restriction posed to the first based on the choice of other one. In our example, the velocity folding is related to the common divisor of the pulse separations, which is equal to 150 μs, corresponding to $\pm$89 m s^{-1}, and the unambiguous range is equal to the period of the repeated code, being equal to 3000 μs or 450 km. It is easy to extend this both ways by choosing longer series of pulses and shorter $\Delta\tau$. The main penalty would be increased computational cost.

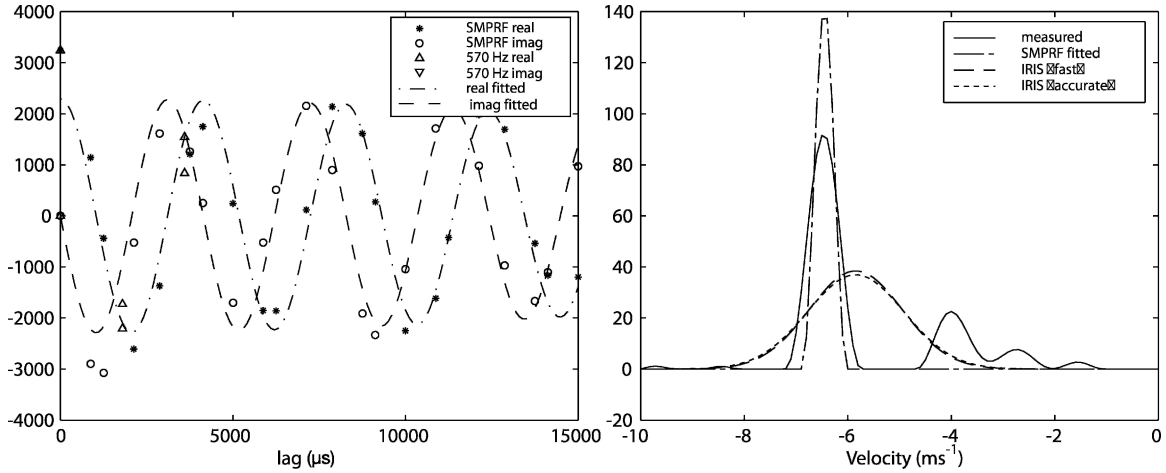

FIG. 11. (left) Measured autocorrelation samples that do not fit to the Gaussian spectrum model, and (right) the corresponding spectrum and spectra of different analysis results.

The results that are shown in this paper indicate that the currently used methods are unable to determine the radar reflectivity at locations with strong ground clutter. The probable reason is the data screening procedure where the IRIS algorithms calculates the ratio of clutter-filtered power to total power at each range gate and according to a user-specified threshold value at which the gate can be rejected (Sigmet, Inc. 2000). The SMPRF solution provides a different approach to the problem of the screening of the results. The clutter power is analyzed as one additional parameter, together with the weather parameters, and the analysis methods provides the distribution function (error estimates) of the unknowns in addition to the most probable values of the unknowns (Lehtinen 1988; Vallinkoski 1988). The screening of the data thus can be based on the user-defined threshold values of the parameter errors. In this way, only the unreliable results are rejected and no unnecessary holes are created.

The SMPRF code produces a large number of autocorrelation samples, which can be used to estimate the spectrum parameters. The present way to analyze the spectrum width is based on the assumption of a Gaussian spectrum shape. However, as is also clearly seen in the spectra shown in this paper, they often look like a sum of two or more Gaussian spectra (probably as a result of wind shear in the scattering region) or may even have a form that is more complicated than that.

Physically, the spectrum shape is closely related to the velocity distribution of the target scattering droplets. It is plausible to suppose that this is a distribution, which is peaked around the average wind velocity and has a shape around that with the spread caused by the atmospheric turbulence. The authors of this paper are no experts on turbulence theories, and, thus, we cannot actually take a position to the question of what kind of velocity distribution would be caused by a typical turbulence structure. Despite this, we think our suspicions about Gaussian shapes are relevant.

More robust estimates of the spectrum parameters can be produced, if the Gaussian spectral theory can be replaced with a more advanced model that allows more freedom in the shape of the spectrum. It is also possible that more advanced raw products than just reflectivity, velocity, and width can be produced with the help of a more advanced spectrum model.

In a future study, we plan to base the analysis on a spectrum model, which assumes the spectrum to be an arbitrary function defined on a support in the Doppler space that is specified by a center frequency and a frequency interval around that. We also plan to generalize this to include a union of two or three intervals like this to be able to handle wind shear situations.

Acknowledgments. The Finnish Meteorological Institute is gratefully acknowledged for providing the IRIS data used in this work. Financial support from Technology Development Centre Finland (Tekes) and the Academy of Finland is gratefully acknowledged.

REFERENCES

Doviak, R. J., and D. S. Zrnić, 1993: *Doppler Radar and Weather Observations*. Academic Press, 562 pp.

Evans, S. N., and P. B. Stark, 2002: Inverse problems as statistics. *Inverse Probl.,* **18,** 55–97.

Farley, D. T., 1972: Multiple-pulse incoherent-scatter correlation function measurements. *Radio Sci.,* **7,** 661–666.

Gray, G., B. Lewis, J. Vinson, and F. Pratte, 1989: A real time implementation of staggered PRT velocity unfolding. *J. Atmos. Oceanic Technol.,* **6,** 186–187.

Greenwald, R. A., K. B. Baker, R. A. Hutchins, and C. Hanuise, 1985: An HF phased-array radar for studying small-scale structure in the high-latitude ionosphere. *Radio Sci.,* **20,** 63–79.

Huuskonen, A., and M. S. Lehtinen, 1996: The accuracy of incoherent scatter measurements: Error estimates valid for high signal levels. *J. Atmos. Terr. Phys.,* **58,** 453–463.

Kaipio, J. P., V. and E. Somersalo, 2004: *Statistical and Computational Inverse Problems*. *Applied Mathematical Sciences*, Vol. 160, Springer-Verlag, 339 pp.

——, V. Kolehmainen, E. Somersalo, and M. Vauhkonen, 2000: Statistical inversion and Monte Carlo sampling methods in electrical impedance tomography. *Inverse Probl.,* **16,** 1487–1522.

Laird, B. G., 1981: On ambiguity resolution by random phase processing. Preprints, *20th Conf. on Radar Meteorology*, Boston, MA, Amer. Meteor. Soc., 327–331

Lehtinen, M. S., 1988: On statistical inversion theory. *Theory and Applications of Inverse Problems*, H. Haario, Ed., Pitman Research Notes in Mathematics Series, Vol. 67, Longman Scientific and Technical, 46–57.

——, 2001: Method and system for measuring radar reflectivity and Doppler shift by means of a pulse radar. U.S. Patent No. 6232913.

——, and I. Häggström, 1987: A new modulation principle for incoherent scatter measurements. *Radio Sci.,* **22,** 625–634.

——, and A. Huuskonen, 1996: General incoherent scatter analysis and GUISDAP. *J. Atmos. Terr. Phys.,* **58,** 435–452.

——, ——, and M. Markkanen, 1997: Randomization of alternating codes: Improving incoherent scatter measurements by reducing correlations of gated ACF estimates. *Radio Sci.,* **32,** 2271–2282.

Mosegaard, K., and M. Sambridge, 2002: Monte Carlo analysis of inverse problems. *Inverse Probl.,* **18,** 29–54.

Pirttilä, J., A. Huuskonen, and M. Lehtinen, 1999: Solving the range-Doppler dilemma with ambiguity-free measurements developed for Incoherent Scatter radars. *COST 75, Advanced Weather Radar Systems, International Seminar, Locarno, Switzerland, 23–27 March 1998,* C. G. Collier, Ed., European Commission, 557–568.

Sachidananda, M., and D. Zrnić, 1999: Systematic phase codes for

resolving range overlaid signals in a Doppler weather radar. *J. Atmos. Oceanic Technol.,* **16,** 1351–1363.

Sigmet, Inc., cited 2000: RVP 7 user's manual. [Available online at ftp://ftp.sigmet.com/outgoing/manuals/rvp7user/.]

Sirmans, D., D. Zrnić, and B. Bumgarner, 1976: Extension of maximum unambiguous Doppler velocity by use of two sampling rates. Preprints, *17th Conf. on Radar Meteorology*, Seattle, WA, Amer. Meteor. Soc., 23–28.

Vallinkoski, M., 1988: Statistics of incoherent scatter multiparameter fits. *J. Atmos. Terr. Phys.,* **50,** 839–851.

——, and M. Lehtinen, 1990: The effect of apriori knowledge on parameter estimation errors with applications to incoherent scatter. *J. Atmos. Terr. Phys.,* **52,** 675–685.

Zrnić, D. S., and P. Mahapatra, 1985: Two methods of ambiguity resolution in pulse Doppler weather radars. *IEEE Trans. Aerosp. Electron. Syst.,* **AES-21,** 470–483.